A through process modeling using multi-assistant software applied to radial fatigue life predication of a 356-T6 wheels

Yongchuan Duan
Yanshan University

Fangfang Zhang (✉ fangfang.zhang@ysu.edu.cn)
Yanshan University

Le Tian
Yanshan University

Yingping Guan
Yanshan University

Jinhua Hu
technical center in CITIC Dicastal limited campany

Original Article

Title page

A through process modeling using multi-assistant software applied to radial fatigue life predication of a 356-T6 wheels

Yong-chuan Duan, born in 1983, is currently a PhD at *Key Laboratory of Advanced Forming & Stamping Technology and Science, Yanshan University, China*. He received his PhD degree from *Yanshan University, China*, in 2014. His research interests include metal material damage and fatigue.
Tel: +86-13253118982; E-mail: yonghcuan.duan @ysu.edu.cn

Fang-fang Zhang, born in 1984, is currently a PhD at *Key Laboratory of Advanced Forming & Stamping Technology and Science, Yanshan University, China*. She received her PhD degree from *Yanshan University, China*, in 2014. Her research interests include damage and fatigue of braided composites.
Tel: +86-13223387868; E-mail: fangfang.zhang @ysu.edu.cn

Le Tian, born in 1993, is currently a master candidate at *Key Laboratory of Advanced Forming & Stamping Technology and Science, Yanshan University, China*.
E-mail: wolfganglele@gmail.com

Ying-ping Guan, born in 1963, is currently a professor at *Yanshan University, China*. He received his PhD degree from *Yanshan Universtiy, China*, in 2000. His research interests include metal material damage and fatigue.
E-mail: gyp@ysu.edu.cn

Jin-hua Hu, born in 1972, is currently a senior engineer at *Technical Center, CITIC Dicastal Limited company, Qinhuangdao 066004, Hebei, China*. His main research interests include metal material damage and fatigue.
E-mail: jinhua@163.com

Corresponding author：Fang-fang Zhang E-mail：fangfang.zhang@ysu.edu.cn

ORIGINAL ARTICLE

A through process modeling using multi-assistant software applied to radial fatigue life predication of a 356-T6 wheels

Yong-chuan Duan[1,2], Fang-fang Zhang[1,2], Le Tian[1,2], Ying-ping Guan[1,2], Jin-hua Hu[3]

Abstract: In order to solve the problem of isolated design in multi-process using multi-assistant software, a through-software radial fatigue life prediction model was established, the effects of shrinkage cavity, SDAS and mean stress on fatigue life were considered. The casting process of the aluminum alloy wheel was simulated based on ProCast, and the data of SDAS and porosity of different parts were predicted based on the solidification process; The data mapping algorithm between tetrahedral mesh elements was developed to realize the unidirectional transformation of microcosmic data from a cast model to a static mechanical model, the radial loading mechanical analysis model of a wheel containing microcosmic information was established; The fatigue life prediction model was established by Fesafe based on the specific mechanical and fatigue parameters of each node. Based on the self-developed TCD software, the integrated coupling method of the three software prediction models was realized. The application of this method on the virtual fatigue prediction experiment of unidirectional tensile specimen reduce the result dispersion between virtual and physical experiment, and the predicted life result error is reduced from 51% to 16%. The proposed method lays a solid foundation of the optimization design and lightweight design of aluminum alloy wheels.

Keywords: Shrinkage cavity SDAS • Mean stress • Data mapping algorithm • Radial fatigue life prediction of wheels

✉ Fang-fang Zhang
   fangfang.zhang @ysu.edu.cn

1 Key Laboratory of Advanced Forming & Stamping Technology and Science, Ministry of Education of China, Yanshan University, Qinhuangdao 066004, Hebei, China

2 College of Mechanical Engineering, Yanshan University, Qinhuangdao 066004, Hebei, China

3 Technical Center, CITIC Dicastal Limited company, Qinhuangdao 066004, Hebei, China

1 Introduction

With the aggravation of global energy problems, the lightweight design methods of auto parts are attracting more attention [1-3]. The improvement of accuracy in predicting service life of auto parts is of great significance to take full advantage of carry capacity, which has been the goal of scholars [4,5]. Wheel before delivery should pass one of the most important radial fatigue test. In order to reduce the design cost and shorten the development cycle, most manufacturers use the virtual experiment method to test the radial fatigue of the wheel before physical experiment, and the prototype design is based on the virtual experiment results [6-8]. However, the results of virtual experiment are deviated from the physical experiment and the predicted results are dispersed, the reliability of the virtual experiment results needs to be improved. In addition, the wheel is not only the important structure part, but also the exterior part of car, only its rear side can be adjusted to meet the corresponding service requirements keeping the appearance of the front side unchanged during the design process. This requirement increases the constraints in the design process, so a fast and reliable radial life prediction method is urgently needed. Many scholars have explored the reasons for the deviation from the results of experiment, casting defects, such as the shrinkage cavity and the SDAS are inevitably introduced into cast aluminum alloy. Roy et al [9] used the experimental method to study the fatigue performance of the material, and found that the defects of the cast aluminum alloy material have great impacts on the formation and propagation of the micro-crack. Gao et al [10] concluded that the fatigue behavior of A356 is determined by the internal defects of the material. Roy et

al [11] found that the fatigue behavior of non-defective cast materials is also affected by SDAS. Gall et al [12] concluded that the fatigue resistance of materials is affected by both microscopic defects and microstructure. Koutiriet et al [13,14] found that the refinement of SDAS can improve the fatigue behavior of materials under cyclic loading, and suggested that Goodman method can be used to consider the impact of mean stress on material fatigue. Mohamed et al [15] studied the effect of defect size on fatigue limit by using Kitigawa diagram.

From the analyses above, the wheel material can not be regarded as homogeneous and invariable, it is necessary to introduce the microstructure and defects of the casting parts into the virtual experiment to eliminate result dispersion [16-18]. Many scholars used a Through Process Modeling (TPM) to predict the fatigue life of parts. P. Li et al [19] used the TPM methodology to predict the fatigue life. Houriaet et al [20] optimized the cast aluminum alloy components by using a TPM methodology. In addition, other finite element methods is proposed to predicate the fatigue, Hidalgo et al [21] predicted the propagation of crack in cast aluminum alloy based on the XFEM, and provided the prediction model of crack initiation and propagation. Vincent et al [22] studied the influence of defect size and shape on fatigue limit based on the coupled FEM and DSG method. Nadot et al [23] used the FEM and Crossland criterion to study the fatigue limit of cast aluminum alloy materials.

Accurate simulation of casting process is important for the prediction of microstructure and microstructure defects, the above scholars used the same mesh and the same analysis software to predict the cooling process of casting parts. However, the cooling process of casting is related on the complex geometry of casting parts and the corresponding casting mold. Casting part geometry includes inlet and other influences parts. It is difficult to simulate accurately of casting cooling history without considering mold, casting geometry and casting process. Thus, many scholars used commercial software such as ProCast to simulate and predict the casting process [24-26]. However, the casting data generated by the software cannot be used through different software. A bridge model need to be built through software by incorporating micro-defects and microstructure data. This model can break the partition of design data between multiple process departments of the enterprise and transmit the design data flow similar to process flow, which is convenient to facilitate the construction of a fully digital factory.

In order to solve the problem of isolated design of multi-assistant software in multi-process, the bridge model of multi-process design data transmission was realized by means of characterization of micro data, and a through software radial fatigue life prediction model of the whole process was formed finally. In this research, the characterization method and algorithm of SDAS and shrinkage cavity data were given first, and the mapping algorithm of SDAS and shrinkage cavity data with mesh correlation was realized through different mesh. Based on the damage theory, the relationship between defect data and mechanical properties was determined, the correlation between defect data and fatigue properties was fitted with the relevant model, and the influences of SDAS, shrinkage cavity data and average stress on fatigue strength were analyzed. The application of this method on the virtual fatigue prediction experiment of unidirectional tensile specimen and wheel radial fatigue can reduce the result dispersion between virtual experiment and physical experiment results.

2   Fatigue life predication method using casting data

In the paper, the fatigue prediction method presented involves three steps. First, the casting and solidification process is simulated by ProCast software, SDAS and shrinkage porosity data of each node are exported from the ProCast model. Second, micro defects and microstructure data are mapped to the element of Abaqus model, and Abaqus is used to analyze the wheel under specific working conditions. Third, micro defects and microstructure data are transmitted to the element of Fesafe model, Fesafe is used to analyze the fatigue of the wheel under specific working conditions, and then the service cycle of the wheel is finally determined. The usage flow is shown in Figure 1.
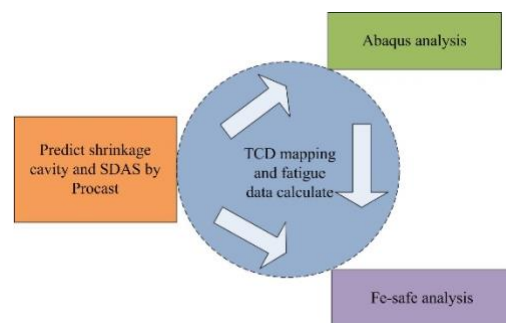
Figure 1 Usage flow of predicated fatigue life tools

2.1 Prediction of SDAS and casting defect based on FEM

SDAS refers to the distance between two adjacent secondary dendrite arms growing on the primary dendrite arm. The study of Li [27] showed that the value of the SDAS is directly related to the alloy composition and local solidification time. In the solidification process of metal, the crystal occurs preferentially where the heat quickly dissipates. SDAS is calculated via Eq.(1):

$$\lambda_2 = 5.5(Mt_s)^n \qquad (1)$$

In the equation, M is the grain coarsening coefficient, n is the grain growth factor, as for A356 aluminum alloy, $M=$ 680μm³/s, and $n= 1/3$.

Through research concluded that, when a liquid phase area is completely contained by the solidified area, the density of the internal material will increase with the decrease of the temperature, and macroscopic shrinkage cavities will be generated at the highest temperature point. The definitions of the shrinkage cavity area and the relevant area are shown in Figure 2, where f_s is the solidification ratio of cast in different area. For the completely solidified area, $f_s=1$, and when the area is liquid, $f_s=0$. As shown in Figure 2, the shrinkage cavity area is located in the area with zero solidification ratio, and the area with zero solidification ratio is contained by the area with one solidification ratio. In mathematical words, it can be expressed as $\Omega_e \subset \Omega_{f_s=0} \subset \Omega_{f_s=1}$.

Generally, macroscopic shrinkage cavity is defined when shrinkage porosity is greater than 1%, and microscopic shrinkage cavity is defined when shrinkage porosity is less than 1%. Shrinkage ratio is calculated via Eq.(2):

$$\varphi_{T-\Delta T}^e = \frac{\rho_T^e}{\rho_{T-\Delta T}^e} \qquad (2)$$

Where, ρ_T^e represents the material density in the area $\Omega_{f_s=0}$ while the temperature is T, $\rho_{T-\Delta T}^e$ represents the material density in the area $\Omega_{f_s=0}$ while the temperature is $T-\Delta T$. In Figure 2, $f_{pif}=0.3$ and $f_{pof}=0.7$.
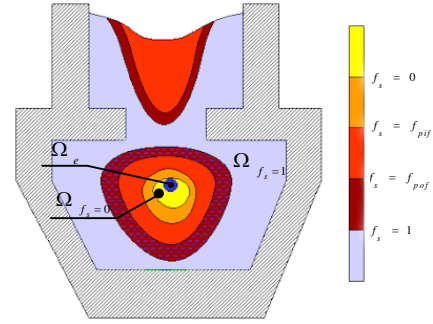
Figure 2 Definition of transformation area from liquid to solidification

The density-temperature curve of A356 aluminum alloy low-pressure cast material is shown in Figure 3. With the decrease of temperature, the accumulative calculation of shrinkage cavity is carried out for each node in the cast model.
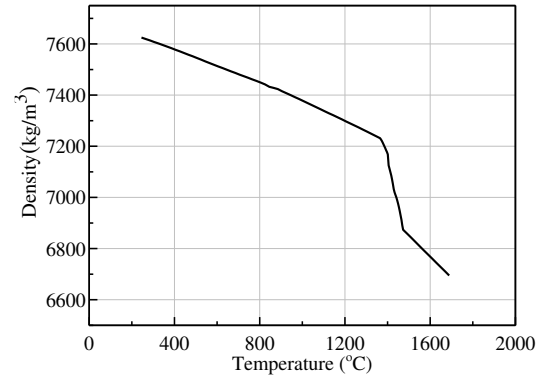

Figure 3 Density-temperature curve of A356 aluminum alloy

2.2 Data mapping algorithm between meshes

Before static analysis and fatigue life prediction, SDAS and shrinkage cavity data of the material should be determined by ProCast. In the casting simulation of the wheel, both the aluminum alloy cast and the cast mold should be discretized. In order to take the effect of cast geometry on the microcosmic properties into full consideration, the geometry of the cast part and the corresponding mould are not simplified. All of these are meshed by tetrahedral elements. Because the temperature drop is very small on the cast and mold contact surface, Shared node mesh transition is adopted on the surface. The cast part is different from the final part, therefore, it is difficult to adopt the same mesh to both the ProCast model and the Abaqus static model. The Abaqus result file is directly imported into the Fesafe for fatigue prediction, so the mesh

of Abaqus static model is exactly same as the Fesafe fatigue prediction model. Machining operations is performed after casting, so the volume of the cast part should be larger than the final part. In order to reduce the difficulty of subsequent mechanical model establishment, the discrete shrinkage cavities and SDAS data on the cast are mapped to the element of Abaqus mechanical model. The micro data mapping algorithm is described as follows.

Suppose that node $P(x, y, z)$ is an arbitrary node in the Abaqus static prediction model [28,29]. we need to find element e that fully contains node P from ProCast model before mapping the result data (including the case of node P on the boundary surfaces and lines of the element). As shown in Figure 4, a typical tetrahedral element has four nodes. Nodes 1, 2, 3 and 4 are the local node number of element e, their sequence meets the right-handed rule. The coordinates of the local nodes in the xyz cartesian coordinate system are respectively (x_1, y_1, z_1), (x_2, y_2, z_3), (x_3, y_3, z_3), (x_4, y_4, z_4). λ_1, λ_2, λ_3 and λ_4 are the SDAS value of the four local nodes, λ_p is the SDAS value of the node P. φ_1, φ_2, φ_3 and φ_4 are the shrinkage porosity of the four local nodes, φ_p is the shrinkage porosity of the node P.
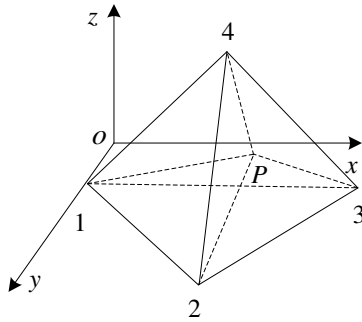
Figure 4 The results of node P extracted from a tetrahedral element

From the node connection and node coordinate file of the ProCast model, the coordinate values of nodes (x_1, y_1, z_1), (x_2, y_2, z_3), (x_3, y_3, z_3) and (x_4, y_4, z_4) are read. Then tetrahedron $P123$, $P234$, $P124$ and $P134$ are constructed by right-handed rule and the volumes of them are calculated by the following expression:

$$V_{1234} = \frac{1}{6} \begin{vmatrix} 1 & x_1 & y_1 & z_1 \\ 1 & x_2 & y_2 & z_2 \\ 1 & x_3 & y_3 & z_3 \\ 1 & x_4 & y_4 & z_4 \end{vmatrix}$$

$$V_{P234} = \frac{1}{6} \begin{vmatrix} 1 & x & y & z \\ 1 & x_2 & y_2 & z_2 \\ 1 & x_3 & y_3 & z_3 \\ 1 & x_4 & y_4 & z_4 \end{vmatrix}$$

$$V_{P134} = \frac{1}{6} \begin{vmatrix} 1 & x_1 & y_1 & z_1 \\ 1 & x & y & z \\ 1 & x_3 & y_3 & z_3 \\ 1 & x_4 & y_4 & z_4 \end{vmatrix} \quad (3)$$

$$V_{P124} = \frac{1}{6} \begin{vmatrix} 1 & x_1 & y_1 & z_1 \\ 1 & x_2 & y_2 & z_2 \\ 1 & x & y & z \\ 1 & x_4 & y_4 & z_4 \end{vmatrix}$$

$$V_{P123} = \frac{1}{6} \begin{vmatrix} 1 & x_1 & y_1 & z_1 \\ 1 & x_2 & y_2 & z_2 \\ 1 & x_3 & y_3 & z_3 \\ 1 & x & y & z \end{vmatrix}$$

Where, V_{P234} is the tetrahedral volume formed by nodes $P234$; V_{P123} is the tetrahedral volume formed by nodes $P123$; V_{P124} is the tetrahedral volume formed by nodes $P124$; V_{P134} is the tetrahedral volume formed by nodes $P134$. When all volume values are greater than or equal to zero, the node P is certainly contained by the element e. When one of the volume values is negative, the node P is certainly not contained by the element e.

Linear interpolation is performed in element e for SDAS and shrinkage porosity via Eq.(4) and Eq.(5) respectively.

$$\lambda_P = L_1 \lambda_1 + L_2 \lambda_2 + L_3 \lambda_3 + L_4 \lambda_4 \quad (4)$$

$$\varphi_P = \varphi_1 \lambda_1 + \varphi_2 \lambda_2 + \varphi_3 \lambda_3 + \varphi_4 \lambda_4 \quad (5)$$

In above equations, L_1, L_2, L_3 and L_4 are the natural coordinate components of element e. The calculation formula of each component is shown in Eq.(6):

$$\begin{cases} L_1 = V_{P432}/V \\ L_3 = V_{P421}/V \\ L_4 = V_{P123}/V \\ L_2 = V_{P413}/V \end{cases} \quad (6)$$

In the equations, V is the total volume value of element e. When the node P coincides with the node 1 of element e, $V_{P234} = V$, $L_1 = 1$, L_2, L_3 and L_4 are equal to zero, and the SDAS of the node P can be entirely obtained by node 1. Similarly, when the node P coincides with node 2, 3 or 4, the SDAS of node P can be entirely obtained by node 2, 3 or 4. When the point P in any other position of element e,

the SDAS of node P is determined by L_1, L_2, L_3 and L_4 together.

The interpolation principle of shrinkage porosity is same as the SDAS calculation. After the shrinkage porosity of any element in the ProCast model being mapped to the Abaqus model, the shrinkage porosity of any node in the Abaqus model can be obtained directly. Define ψ_{i1}, ψ_{i2}, ψ_{i3} and ψ_{i4} as the shrinkage porosity of each local node of element i in Abaqus model, ψ_i is the average shrinkage porosity of element i, the formula is shown in Eq.(7).

$$\psi_i = (\psi_{i1} + \psi_{i2} + \psi_{i3} + \psi_{i4})/4 \tag{7}$$

Shrinkage cavity defect sizes can be characterized by $\sqrt{area}$ [23]. It is defined as the square root of the projected area on the plane perpendicular to the direction of the maximal principal stress of the defect. When the shrinkage cavity type of element i is spherical, $\sqrt{area}$ can be calculated based on element volume via Eq.(8):

$$\sqrt{area} = \sqrt[6]{\frac{9\pi\psi_i^2 V_i^2}{16}} \tag{8}$$

In the equation, V_i is the volume of element i. The test model mapping results from casting to part are show as Figure 5:
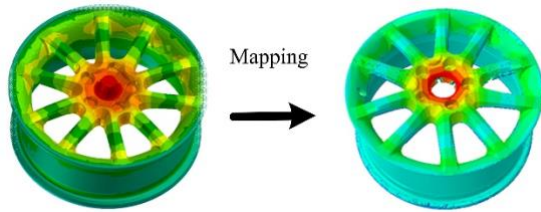

Figure 5 The mapping results from casting to part

2.3 The predication of relationship between stress amplitude and fatigue life using casting data

Houria [15] thought that the yield stress is related to SDAS in casting microstructure, and the relationship between yield stress and SDAS is given in Eq.(9).

$$\sigma_s = \sigma_0 \exp(-\frac{\lambda_2}{\lambda_0}) \tag{9}$$

For A356 aluminum alloy, $\lambda_0 = 244\mu m$, $\sigma_0 = 278 MPa$.

In the static calculation, the linear elastic relation is satisfied in the elastic phase, the yield stress at the end of elastic phase is calculated by Eq.(9). The hardening curve

beyond the yield point is simplified as a straight line. Based on damage mechanics theory, when the shrinkage cavities appear in the material, the damage variable can be expressed by the shrinkage rate ψ, so we define the damage variable as the ratio of the shrinkage cavity area to the original area. This paper focuses on the high cycle fatigue behavior of the cast aluminum alloy, and the stress inside the part is relatively small, therefore, it is assumed that the hardening rate is independent of the material microstructure. In summary, the constitutive equations of the material are expressed as follow:

$$\sigma = \begin{cases} E(\psi)\varepsilon & \varepsilon \le \varepsilon_0 \\ \sigma_s(\lambda_2) + D(\varepsilon - \varepsilon_0) & \varepsilon \ge \varepsilon_0 \end{cases} \tag{10}$$

$$\varepsilon_0 = \sigma_s(\lambda_2)/E(\psi) \tag{11}$$

Reference [15] assumed that fatigue limit σ_D is a quadratic function of SDAS and $\sqrt{area}$, and response surface method is used to fit correlation coefficients of this function under 10^6 cycles at R=-1. The relationship between fatigue limit and microscopic parameters is shown as Eq.(12):

$$\sigma_D = A \times SDAS^2 + B \times \sqrt{area}^2 \\ + C \times SDAS \times \sqrt{area} + D \tag{12}$$

A, B, C and D are the coefficients of the material which need to be determined. They will be fitted by the experimental data.

The mean stress has a significant effect on the fatigue life. The relationship between mean stress and fatigue limit is described based on Goodman iso-life curve. The Goodman curve equation is shown as Eq.(13):

$$\frac{S_a}{S_{-1}} + \frac{S_m}{S_u} = 1 \tag{13}$$

S_{-1} is the fatigue limit of the material with the stress ratio R=-1. Under the condition of different SDAS and shrinkage size, $S_{-1} = \sigma_D$. S_u is the fracture strength of the material. S_a can represent the fatigue limit under mean stress S_m condition. The relationship between stress ratio R and mean stress S_m is shown as Eq.(14):

$$S_m = (1+R)S_a/(1-R) \tag{14}$$

Substitute Eq.(13) into Eq.(14), stress ratio R is obtained as :

$$R = \frac{S_m - S_{-1} + S_{-1}S_m / S_u}{S_m + S_{-1} - S_{-1}S_m / S_u} \qquad (15)$$

Suppose the *S-N* curve of the material is in the form of power function [30], it is expressed as Eq.(16):

$$S^m N = C \qquad (16)$$

Two coefficients of the power function can be obtained by substituting two coordinate points $\left(S_a, 10^6\right)$ and $(S_u, 1)$ of *S-N* curve into Eq.(16):

$$m = \frac{6}{\log_{10}(S_u) - \log_{10}(S_a)} \qquad (17)$$

$$C = S_u^{\ m} \qquad (18)$$

The yield stress and elastic modulus of the material at different SDAS and shrinkage porosity can be obtained by the method, and also the *S-N* curves under different SDAS, shrinkage rate and *R*. Then the *S-N* curve and the mechanical properties will be used to predict the total life of one part.

3 Verification of fatigue life prediction algorithm by uniaxial tensile test

In order to verify the correctness of the method, the cast model shown in Figure 6 is established. The cast is a wedge block. The upper part of the mold cavity is wide and the lower part is narrow, so different solidification time can be obtained in the direction of the wedge height, and different SDAS values can also be generated. Tensile specimens are cut from different positions in the direction of the wedge block height. There are 8 specimens from the bottom to the top, numbered as 2~9 respectively, as shown in Figure 6. The experiment data from literature [15] of these specimens 2~9 are listed in the Table 1. The numbered 1 specimen for subsequent analysis is cut from the spoke position of the wheel. ProCast is used to simulate the casting process of wedge, and the results are in good agreement with the literature [15]. The nephogram of SDAS is shown in Figure 7(a). The specific height and correspond SDAS are shown in Table1. There is no shrinkage porosity higher than 1%, and the whole performance is micro-shrinkage and does not change much at different heights. Therefore, no additional numerical comparison is given in Table 1.
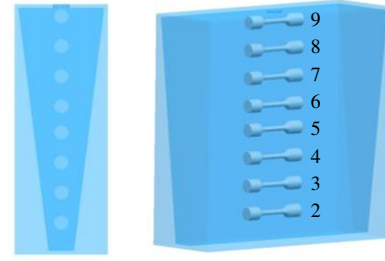
Figure 6 The location of fatigue specimens extracted from a wedge casting
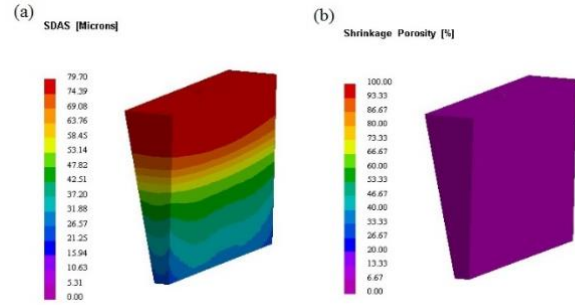
Figure 7 Predicated SDAS and shrinkage porosity contour results for the wedge casting: (a) Predicated SDAS contours of the wedge casting; (b) Predicated shrinkage porosity contours of the wedge casting

It can be seen from the simulation results that the SDAS value of cast increases with the increasing of the distance to the wedge bottom. The shrinkage porosity barely changes and is shown in Figure 7(b). The uniaxial tensile model and uniaxial tensile fatigue life prediction model with microscopic data are obtained by mapping the SDAS and the shrinkage porosity at different locations. The results of uniaxial tensile fatigue test and simulation prediction are shown in Table 1, The maximum prediction error of fatigue limit is 12.82%.

4 Verification of fatigue life prediction algorithm by the aluminum alloy wheel test

### 4.1 Establishment of cast model and prediction of micro-data

In the actual casting process of a wheel, a certain gas pressure is applied to the alloy liquid surface in the sealed furnace. Under the pressure, the molten metal is filled into the mould through the lift tube at bottom, as shown in Figure 8. After the metal in the cavity is completely solidified, the lateral die is opened and the top die is lifted vertically, then the mandril will push the formed wheel out from the bottom die to complete a casting cycle. The

**Table 1** Comparison of tensile test results and simulated data

| Family	Number	Distance to the top(mm)	Experiment SDAS (μm)	Predicated SDAS (μm)	Experiment fatigue limit (MPa)	Predicated fatigue limit (MPa)	Error %
From wheel	1	N/A	39 ± 9.2	39.5 ± 2.6	91.939	90.913	1.12
Wedge bottom	2	28	39.5 ± 7.6	35.2±5.9	91.779	91.253	0.57
	3	58	39.7 ± 9.1	37.6±6.9	91.714	90.062	1.80
	4	88	47.6 ± 14.1	44.1±5.7	88.891	88.010	0.99
Wedge middle	5	118	57.2 ± 17.9	51.5±4.5	84.744	85.306	0.66
	6	144	58.5 ± 21	64.8±5.6	84.122	77.761	7.56
	7	174	59.7 ± 21.2	75.5±2.4	83.536	73.131	12.46
Wedge top	8	204	62.6 ± 21.6	78.6±1.7	82.067	71.549	12.82
	9	234	72.2 ± 28.2	79.2±2.1	76.693	70.875	7.59

ProCast is used to simulate the metal filling process. In the simulation, the gas pressure and pouring speed are consistent with that of the actual pouring process at the inlet.
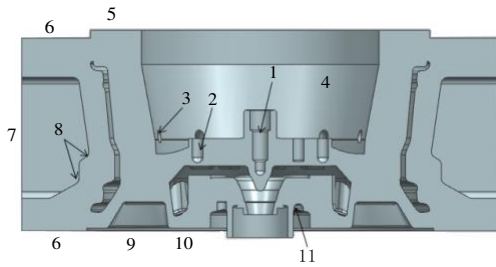
Figure 8 Cast mould for the aluminum alloy wheel with different convective heat transfer settings

To ensure the cast being orderly solidified, different convective heat transfer coefficient are applied to different parts of the mould. The following optimal heat emission condition were adopted in the factory. The convective heat transfer coefficient 5000W/(m2k) used for water cooling condition was applied at 1; the convective heat transfer coefficient 600W/(m2k) used for wind cooling condition was applied at 2, 3, 8 and 10 respectively; the convective heat transfer coefficient 10W/(m2k) used for air cooling condition was applied at remained outside surfaces. The SDAS distribution of cast part is shown in Figure 9(a). In the process of cast, the heat dissipation area at the rim is bigger, so the solidification time is shorter, thus the SDAS is smaller. The place where the spokes closed to the wheel center, contains more heat and has poor cooling conditions, so the solidification time of it is longer and the dendrites grows fully in it, so the SDAS is large. The contours of shrinkage porosity greater than 1% are given by the post processing program, as shown in Figure 9(b). According to the heat dissipation and solidification process of the wheel, we found that the spokes and rims are solidified firstly. The connection area between spoke and rim and between spoke and the wheel center do not reach the critical solid fraction at the same time. This area forms a closed liquid-phase area and cannot be feed by materials from other area. According to the forming conditions of shrinkage cavities, casting defects such as shrinkage cavity are likely to be produced in this area. According to Figure 9(b), the area of the spokes closed to the wheel center has the highest shrinkage porosity, and small defects also occur at the rim.
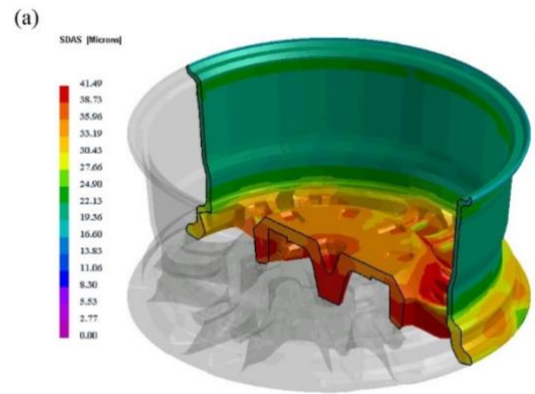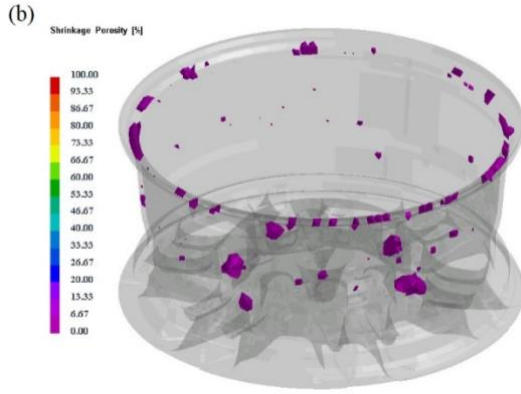
Figure 9 Predicated SDAS and shrinkage porosity contour results for the wheel: (a) Predicated SDAS contours of the wheel; (b) Predicated shrinkage porosity contours of the wheel

4.2 Establishment of radial loading static model

The wheel radial fatigue test platform is mainly composed of drum and installation shaft. The drum is driven by electric motor. The installation shaft can be moved in the radial direction of the drum to provide a radial force. The wheel is driven by the friction between the drum and the tire [31]. In order to accelerate the life evaluation, the radial load in the actual test is scaled according to Eq.(19).

$$F_r = F_v K \qquad (19)$$

F_v is the rated load of the wheel, $F_v=22175$. K is the strengthening coefficients, $K=2.0$.

In the simulation of radial fatigue test, the radial load is transferred to the wheel through the tire. The tire mounted on the wheel can disperse the applied radial load. To ensure the accurate prediction of the stress field, actual model is used. Hyper elastic material is used to establish the tire. Bead wire is established by linear elastic material on the edge of the tire. The contact between tire rim wire and tire rubber is established, and also that between the wheel and the tire. The contact surfaces of the two group contacts are shown in Figure 10. The internal pressure is applied on the inner surface of the sealing cavity formed by the tire and rim.
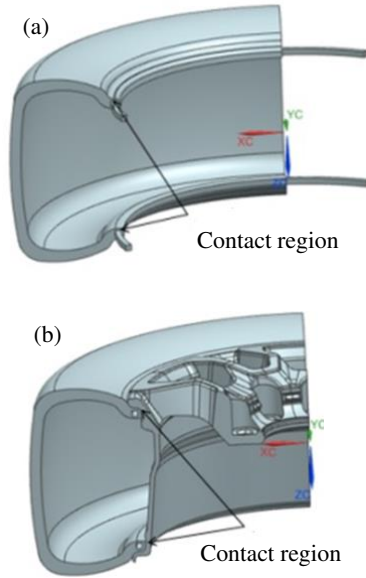
Figure 10 All contact pairs between the tire and the wheel: (a) Contact between the tire and the rim wire; (b) Contact between the tire and the wheel

The wheel and drum continuously rotate under the specified load. To realize the discrete calculation of the FEM, the continuous process is simplified as 12 discrete loads sequentially loaded [32,33]. In the Abaqus model, 13 load steps are set, and a loading in one direction is finished by 2 load steps, the previous load step is used for loading, and the latter load step is used for unloading. The loading diagram is shown in Figure 11.
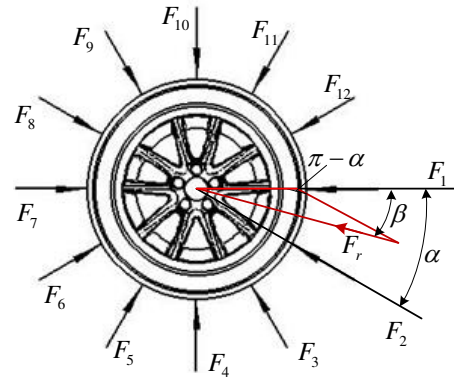

Figure 11 Load schematic diagram for radial fatigue test

loading and unloading are executed in the order of F_1-F_{12}. For example, while the wheel is rotating between F_1 and F_2, the force at rotated angle β is F_r. This constant amplitude force at any angle can be constructed by adjusting the magnitudes of force at direction of F_1 and F_2. The magnitude parametric equations of load applied in the

direction of F_1 and F_2 are shown as follows:

$$
\begin{cases}
t_3 = \beta/\alpha + 2 \\
A_1 = \sin\beta/\cos\alpha \\
A_2 = \sin(\alpha - \beta)/\cos\alpha
\end{cases}
\tag{20}
$$

A_1 and A_2 are amplitudes of load in F_1 and F_2 direction respectively. When the wheel is rotating between other load pairs, the corresponding load amplitude can be obtained in the same way. The amplitude curves applied by the model in different load directions are shown in Figure 12. Step-1 is used for apply F_n and tire internal pressure P. Step-2 and step-n have periodicity, a cycle is composed of step-2 to step-n.
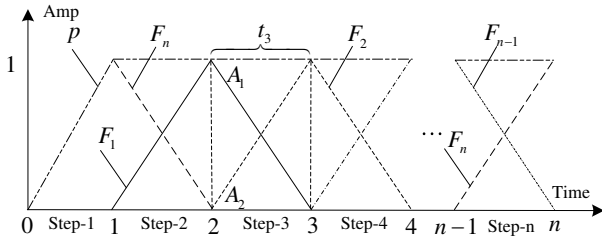

Figure 12 Sequence diagram of amplitudes for different loads direction

4.3 Establishment of radial fatigue model

The static analysis results from Abaqus software are imported into Fesafe [34-36]. 12 datasets are imported as a data group into the "Elastic Block" in Fesafe. The fatigue algorithm calculates the fatigue life of each node by the fatigue software. The inherited microscopic data need to be converted into fatigue data by TCD software at each node. The S-N curves with different defect sizes, different SDAS and different mean stresses can be constructed by the above algorithm. The stress amplitude surface can be obtained by superimposing the family of curves under different conditions, it is shown in Fig.12. In order to facilitate the analysis, an axis is scaled from the number of cycles to its logarithmic value. Figure 13(a) is the stress amplitude surface under different number of cycles, different SDAS values and different mean stresses, when the $\sqrt{area}$ is set at 450um. The three surfaces are stress amplitude surfaces when the mean stress is 0, 30 and 60 respectively. As seen from the figure, with the increase of the mean stress, the stress amplitude surface moves down, and the offset distance is almost same. From the contours in the figure, it can be concluded that the fatigue life decreases with the increase of SDAS. Figure 13(b) shows the influence of

SDAS on stress amplitude with the same life. As SDAS increases, stress amplitude decreases gradually. Figure 13(c) is the stress amplitude surface under different number of cycles, different $\sqrt{area}$ and different mean stresses when the SDAS value is set at 50. The three surfaces are the stress amplitude surfaces when the mean stress is 0, 30 and 60 respectively. From the isoheight line in the figure, it can be concluded that when $\sqrt{area}$ is less than 400um, the stress amplitude decreases with the increases of $\sqrt{area}$, but the decrease is small; when the $\sqrt{area}$ value is more than 400um, the stress amplitude shows a large nonlinear reduction. Figure 13(d) shows the influence of different shrinkage cavity sizes on stress amplitude with the same life. With the increase of shrinkage cavity size, stress amplitude gradually decreases, and the decreasing trend is similar to the life. Through the above analysis, we can see that the SDAS of cast aluminum alloy material is greatly affected by the solidification time. In order to improve the fatigue life of the parts, the cooling rate of different parts should be adjusted as large as possible. Micro shrinkage is inevitable in casting process. When $\sqrt{area}$ is less than 400um, the fatigue life of the material is reduced slightly, but the material is sensitive to macroscopic shrinkage defects exceeding 400um. The surface data are discretized as the fatigue database file of each node, and are imported to Fesafe to complete the property setting of the fatigue model.
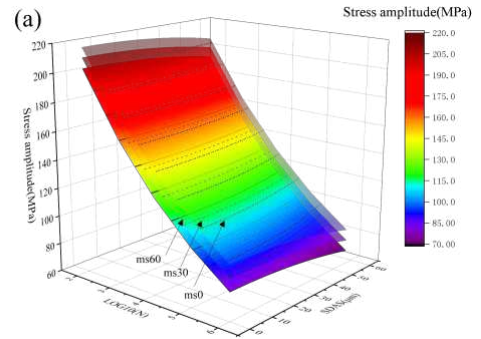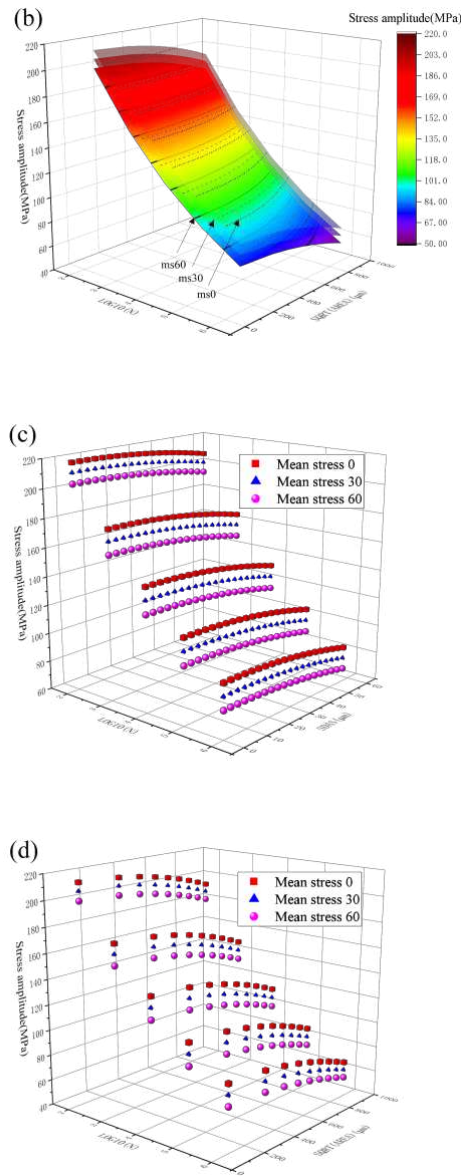
Figure 13 Stress amplitude and fatigue life with SDAS and shrinkage cavity size at different mean stress level: (a) Stress amplitude with SDAS and fatigue life at different mean stress level; (b) Stress amplitude with shrinkage cavity size and fatigue life at different mean stress level; (c) Stress amplitude with SDAS at different fatigue life level and mean stress level; (d) Stress amplitude with shrinkage cavity size at different fatigue life level and mean stress level

4.4 Results and analysis

The result file that can be recognized by commercial software is produced after the fatigue model being submitted for calculation. In the paper, the fatigue output file is imported into the Abaqus CAE environment for post-processing analysis. The fatigue life contours of the wheel under radial load is shown in Figure 14.

From the results of fatigue simulation analysis, it can be seen that the fatigue life of the connection area between spoke and the wheel center is the lowest in the radial fatigue test. The fatigue crack appears first in this area. The area mentioned above is the dangerous area of the wheel. In the simulation analysis of radial fatigue test, the predicted locations of the minimum fatigue life are all in the connection area between the spokes and the wheel center, both with and without considering the casting defects. But in the simulation analysis of fatigue test considering the casting defects, the minimum fatigue life appears on the outside of the two connected spokes, as shown in Figure 14(b). The minimum fatigue life is $10_{5.93}$, which is about 0.84 million. In the fatigue life simulation analysis without considering casting defects, the minimum fatigue life appeared on the inside of two connected spokes, and the minimum fatigue life is $10_{6.18}$, which is about 1.51 million. The average fatigue life of first batch measured by physical experiments on multiple wheels is 1.00 million. The average fatigue life of second batch measured by physical experiments on multiple wheels is 0.94 million, the location of minimum fatigue life is shown in Figure 15. By comparing the results of fatigue life prediction considering casting defects, it can be seen that the influence of microcosmic effect is small on fatigue location prediction, and is larger on fatigue life prediction. The fatigue life prediction becomes more accurate when the casting defects are taken into consideration.
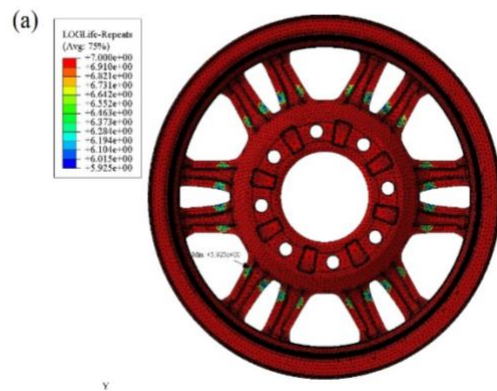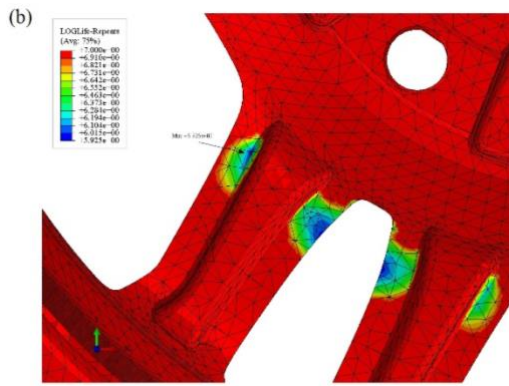
Figure 14 Predicated fatigue life contours of the wheel radial test considering casting defects: (a) fatigue life contours on the back of the wheel; (b) Enlarged view of the min fatigue life region

Figure 15 Location of the minimum fatigue life obtained from the wheel fatigue test

5   Conclusions

(1) A multiscale fatigue prediction method considering shrinkage cavity, SDAS and mean stress level of cast aluminum alloy materials is proposed. The data mapping algorithm between tetrahedral mesh elements is developed, and the unidirectional transmission of microcosmic data from casting FEM results to Abaqus static model is realized. The integrated coupling of the three software prediction models is realized based on the self-developed TCD software. And the precise prediction of radial fatigue life of a wheel is realized while the shrinkage cavity, SDAS and mean stress level are taken into consideration.

(2) The fatigue simulation and the fatigue test are proceeded for the uniaxial tensile specimens cut from different heights in the wedge block. By comparing the simulation results with fatigue test results, the fatigue prediction method is verified. The results show that the fatigue prediction method has a good accuracy, and the maximum predicated error is 12.82%.

(3) Based on the node mechanics properties and fatigue parameter calculation method presented in this paper, it is concluded that the stress amplitude decreases with the increase of SDAS. When the $\sqrt{area}$ is less than 400um, the fatigue life slightly decreases. When the $\sqrt{area}$ value reaches about 400um, the stress amplitude shows a large nonlinear reduction. The material is sensitive to macroscopic shrinkage defects exceeding 400um.

(4) The radial fatigue simulation of an aluminum alloy wheel is established based on the fatigue prediction method proposed in the paper. Compared with the results of traditional fatigue life prediction method without considering defects and physical experiment, the new results show that the influence of microscopic effect on the fatigue position prediction is small, and the influence on the fatigue life is larger. Predicated life is more accurate.

6   Declaration

Availability of data and materials
The datasets supporting the conclusions of this article are included within the article.

Authors' contributions
The author' contributions are as follows: Yong-chuan Duan was in charge of the whole trial; Yong-chuan Duan wrote the manuscript; Le Tian, Fang-fang Zhang and Jin-hua Hu assisted with sampling and laboratory analyses. Ying-ping Guan gives the advices about the manuscript.

Competing interests
The authors declare no competing financial interests.

Consent for publication
Not applicable

Ethics approval and consent to participate

Not applicable

References

[1] CHAI W H, LIU X D, SHAN Y C, WAN X F, JIANG E. Research on simulation of the bending fatigue test of automotive wheel made of long glass fiber reinforced thermoplastic considering anisotropic property[J]. *Advances in Engineering Software*, 2018, 116:1-8.

[2] SPANGENBERGER A G, LADOS D A, COLEMAN M, BIROSCA S, MARK C. Microstructural mechanisms and advanced characterization of long and small fatigue crack growth in cast A356-T61 aluminum alloys[J]. *International Journal of Fatigue*, 2017, 97:202-213.

[3] ROTELLA A, NADOT Y, PIELLARD M, AUGUSTIN R, FLEURIOT M. Fatigue limit of a cast Al-Si-Mg alloy (A357-T6) with natural casting shrinkages using ASTM standard X-Ray inspection[J]. *International Journal of Fatigue*, 2018, 114.

[4] BRUDER T, HANSELKA H, HEIM R, KAUFMANN H. Fatigue and structural durability of automotive components[J]. *Road and Off-Road Vehicle System Dynamics Handbook*, 2014, 1708.

[5] SONG, PARK, JEONG, AHN. Fatigue behaviour of A356 aluminium alloy for automotive wheels[J]. *International Journal of Cast Metals Research*, 2012, 25(1).

[6] WAN X F, SHAN Y C, LIU X D, WANG H X, WANG J G. Simulation of biaxial wheel test and fatigue life estimation considering the influence of tire and wheel camber[J]. *Advances in Engineering Software*, 2016, 92:57-64.

[7] FABIO M S, RICCARDO M, IVO K, FRANCO G D. Simulation of the scenario of the biaxial wheel fatigue test[J]. *Advances in Engineering Software*, 2017, 114:337-347.

[8] BAEKER M, GALLREIN A, CALEBRESE F, CIBRARIO V. SIMULATION—Simulation of a tire blow-out in a full vehicle scenario[M]. *7th International Munich Chassis Symposium* 2016, 2017, 869:98.

[9] ROY M, NADOT Y, MAIJER D M, BENOIT G. Multi axial Fatigue Behaviour of A356-T6[J]. *Fatigue & Fracture of Engineering Materials & Structures*, 2014, 35(12).

[10] GAO Y X, YI J Z, LEE P D, LINDLEY T C. A micro-cell model of the effect of microstructure and defects on fatigue resistance in cast aluminum alloys[J]. *Acta Materialia*, 2004, 52(19):5435-5449.

[11] ROY M J, NADOT Y, NADOT M C, BARDIN P G, MAIJER D M. Multiaxial Kitagawa analysis of A356-T6[J]. *International Journal of Fatigue*. 2011, 33(6):823-32.

[12] GALL K, YANG N, HORSTEMEYER M, MCDOWELL, FAN X G. The influence of modified intermetallics and Si particles on fatigue crack paths in a cast A356 Al alloy[J]. *Fatigue & Fracture of Engineering Materials & Structures*, 2000, 23(2):159-172.

[13] KOUTIR I, BELLETT D, MOREL F, AUGUSTINS L, ADRIEN J. High cycle fatigue damage mechanisms in cast aluminium subject to complex loads[J]. *International Journal of Fatigue*, 2013, 47:44-57.

[14] KOUTIR I, BELLETT D, MOREL F, PESSARD E. A probabilistic model for the high cycle fatigue behaviour of cast aluminium alloys subject to complex loads[J]. *International Journal of Fatigue*, 2013, 47:137-47.

[15] HOURIA M I, NADOT Y, FATHALLAH R, ROY M, MAIJER D M. Influence of casting defect and SDAS on the multiaxial fatigue behaviour of A356-T6 alloy including mean stress effect[J]. *International Journal of Fatigue*, 2015, 80:90-102.

[16] LEE C D, YOO S J. Dependence of fatigue life of low-pressure die-cast A356 aluminum alloy on microporosity variation[J]. *Metals and Materials International*, 2014, 20(4):601-612.

[17] AMMAR H R, SAMUEL A M, SAMUEL F H. Effect of casting imperfections on the fatigue life of 319-F and A356-T6 Al-Si casting alloys[J]. *Materials Science & Engineering A (Structural Materials: Properties, Microstructure and Processing)*, 2007, 473(1-2):65-75.

[18] DONG S Y, ZHUANG Z, XU Q Y, XIONG S M, LIU B C. Preliminary study on simulation of microporosity evolution and fatigue life of aluminum alloy casting[J]. *International Journal of Cast Metals Research*, 2003, 15(4).

[19] LI P, MAIJER D M, LINDLEY T C, LEE P D. A through process model of the impact of in-service loading, residual stress, and microstructure on the final fatigue life of an A356 automotive wheel[J]. *Materials Science and Engineering A, Structural Materials: Properties, Microstructure and Processing*, 2007, 61:20-30.

[20] HOURIA M I, NADOT Y, FATHALLAH R, MAIJER D M, GORGE A L. Through process modeling applied to the fatigue design of cast A356-T6 components[J]. *Engineering Fracture Mechanics*, 2018, 195:267-278.

[21] HIDALGO R, ESNAOLA J A, LLAVORI I, LARRANAGA M, HURTADO I, DORCA N H. Fatigue life estimation of cast aluminium alloys considering the effect of porosity on initiation and propagation phases[J]. *International Journal of Fatigue*, 2019, 125:468-478.

[22] VINCENT M, NADOT M C, NADOT Y, DRAGON A. Fatigue from defect under multiaxial loading: Defect Stress Gradient (DSG) approach using ellipsoidal Equivalent Inclusion Method[J]. *International Journal of Fatigue*, 2014, 59:176–187.

[23] BILLAUDEAU T, NADOT Y, BEZINE G. Multiaxial fatigue limit for defective materials: mechanisms and experiments[J]. *Acta Materialia*, 2004, 52(13):3911-3920.

[24] ZHANG G Y, JING T, LIU B. Microstructure simulation of aluminum alloy casting using phase field method[J]. *International Journal of Cast Metals Research*, 2016.

[25] HAN X , ZHANG H T, SHAO B, WANG D T, CHENG L G, GUO Y D, QIN K, CUI J Z. Numerical simulation on sprue distributions during cladding casting process[J]. *International Journal of Numerical Methods for Heat & Fluid Flow*, 2016, 26(8):2340-2354.

[26] ZHANG S Y, XU Z F, WANG Z T. Numerical modeling and simulation of water cooling controlled solidification for aluminum alloy investment casting[J]. *International Journal of Advanced Manufacturing Technology*, 2017, 91(1-4).

[27] LI B, SHEN Y, HU W. Casting defects induced fatigue damage in aircraft frames of ZL205A aluminum alloy -A failure analysis[J]. *Materials and Design*, 2011, 32(5):2570-2582.

[28] KONRAD S, BENJAMIN K, SWANTJE B. Automatic three-dimensional geometry and mesh generation of periodic representative volume elements for matrix-inclusion composites[J]. *Advances in Engineering Software*, 2016, 99.

[29] LINA R, YOANN J. An Abaqus ™ plug-in for the geometry generation of Representative Volume Elements with randomly distributed fibers and interphases[J]. *Composite Structures*, 2019, 209.

[30] LI P, ZHANG G D, XU C. Study on determination method of high cycle stress fatigue S-N curve[J]. *Gas Turbine Test and Research*, 2008, 21(2):39-43.

[31] AYKUT C, MAHMUT D, CUNEYT A, RAMAZAN A, AHMET A, GUSAN H, ERGUN T, OZKARDESLER B C. Wheel Hub Fatigue Performance under Non-constant Rotational Loading and Comparison to Eurocycle Test[J]. *Procedia Engineering*, 2015, 101.

[32] WANG X, ZHANG X. Simulation of dynamic cornering fatigue test of a steel passenger car wheel[J]. *International Journal of Fatigue*, 2010, 32(2):434-442.

[33] TOPAC M M, ERCAN S, KURALAY N S. Fatigue life prediction of a heavy vehicle steel wheel under radial loads by using finite element analysis[J]. *Engineering Failure Analysis*, 2011, 20.

[34] NESLADEK M, SPANIEL M. An Abaqus plugin for fatigue predictions[J]. *Advances in Engineering Software*, 2017, 103:1-11.

[35] ANDY M K. Multiscale composite analysis in Abaqus: Theory and motivations[J]. *Reinforced Plastics*. 2017, 61(3):153–6.

[36] HACHEMI M E, KOUTSAWA Y, NASSER H, GIUNTA G, DAOUADJI A, DAYA E M, BEIOUETTAR S. Anintuitive computational multi-scale methodology and tool for the dynamic modelling of viscoelastic composites and structures. *Compos Struct .* 2016, 144:131–7.

Biographical notes

Yong-chuan Duan, born in 1983, is currently a PhD at *Key Laboratory of Advanced Forming & Stamping Technology and Science, Yanshan University, China*. He received his PhD degree from *Yanshan University, China*, in 2014. His research interests include metal material damage and fatigue.
Tel: +86-13253118982; E-mail: yonghcuan.duan@ysu.edu.cn

Fang-fang Zhang, born in 1984, is currently a PhD at *Key Laboratory of Advanced Forming & Stamping Technology and Science, Yanshan University, China*. She received her PhD degree from *Yanshan University, China*, in 2014. Her research interests include damage and fatigue of braided composites.
Tel: +86-13223387868; E-mail: fangfang.zhang @ysu.edu.cn

Le Tian, born in 1993, is currently a master candidate at *Key Laboratory of Advanced Forming & Stamping Technology and Science, Yanshan University, China.*
Tel: +86-17736373668; E-mail: wolfganglele@gmail.com

Ying-ping Guan, born in 1963, is currently a professor at *Yanshan University, China*. He received his PhD degree from *Yanshan Universtiy, China*, in 2000. His research interests include metal material damage and fatigue.
E-mail: gyp@ysu.edu.cn

Jin-hua Hu, born in 1972, is currently a senior engineer at *Technical Center, CITIC Dicastal Limited company, Qinhuangdao 066004, Hebei, China.* His main research interests include metal material damage and fatigue.
E-mail: jinhua@163.com

Appendix

Appendix and supplement both mean material added at the end of a book. An appendix gives useful additional information, but even without it the rest of the book is complete: In the appendix are detailed charts. A supplement, bound in the book or published separately, is given for comparison, as an enhancement, to provide corrections, to present later information, and the like: A yearly supplement is issue.